Am J Physiol Gastrointest Liver Physiol 320: G644–G657, 2021.
First published February 3, 2021; doi:10.1152/ajpgi.00363.2020

american physiological society

AMERICAN JOURNAL OF PHYSIOLOGY
GASTROINTESTINAL AND LIVER PHYSIOLOGY

RESEARCH ARTICLE

Neurogastroenterology and Motility

Optical clearing reveals TNBS-induced morphological changes of VGLUT2-positive nerve fibers in mouse colorectum

Tiantian Guo,[1] Shivam Patel,[2] Dhruv Shah,[3] Ling Chi,[2] Sharareh Emadi,[1] David M. Pierce,[1,4] Martin Han,[1] Pablo R. Brumovsky,[5] and Bin Feng[1,2]

[1]*Department of Biomedical Engineering, University of Connecticut, Mansfield, Connecticut;* [2]*Department of Physiology and Neurobiology, University of Connecticut, Mansfield, Connecticut;* [3]*Department of Molecular and Cell Biology, University of Connecticut, Mansfield, Connecticut;* [4]*Department of Mechanical Engineering, University of Connecticut, Mansfield, Connecticut; and* [5]*Instituto de Investigaciones en Medicina Traslacional, National Scientific and Technical Research Council, Austral University, Buenos Aires, Argentina*

Abstract

Colorectal hypersensitivity and sensitization of both mechanosensitive and mechanically insensitive afferents develop after intracolonic instillation of 2,4,6-trinitrobenzenesulfonic acid (TNBS) in the mouse, a model of postinfectious irritable bowel syndrome. In mice in which ~80% of extrinsic colorectal afferents were labeled genetically using the promotor for vesicular glutamate transporter type 2 (VGLUT2), we systematically quantified the morphology of VGLUT2-positive axons in mouse colorectum 7–28 days following intracolonic TNBS treatment. After removal, the colorectum was distended (20 mmHg), fixed with paraformaldehyde, and optically cleared to image VGLUT2-positive axons throughout the colorectal wall thickness. We conducted vector path tracing of individual axons to allow systematic quantification of nerve fiber density and shape. Abundant VGLUT2-positive nerve fibers were present in most layers of the colorectum, except the serosal and longitudinal muscular layers. A small percentage of VGLUT2-positive myenteric plexus neurons was also detected. Intracolonic TNBS treatment significantly reduced the number of VGLUT2-positive nerve fibers in submucosal, myenteric plexus, and mucosal layers at *day 7* post-TNBS, which mostly recovered by *day 28*. We also found that almost all fibers in the submucosa were meandering and curvy, with ~10% showing pronounced curviness (quantified by the linearity index). TNBS treatment resulted in a significant reduction of the proportions of pronounced curvy fibers in the rectal region at 28 days post-TNBS. Altogether, the present morphological study reveals profound changes in the distribution of VGLUT2-positive fibers in mouse colorectum undergoing TNBS-induced colitis and draws attention to curvy fibers in the submucosa with potential roles in visceral nociception.

NEW & NOTEWORTHY We conducted genetic labeling and optical clearing to visualize extrinsic sensory nerve fibers in whole-mount colorectum, which revealed widespread presence of axons in the submucosal layer. Remarkably, axons in the submucosa were meandering and curvy, in contrast to axons in other layers generally aligned with the basal tissues. Intracolonic TNBS treatment led to pronounced changes of nerve fiber density and curviness, suggesting nerve fiber morphologies as potentially contributing factors to sensory sensitization.

afferent sensitization; channelrhodopsin; colorectum; optical tissue clearing; VGLUT2-Cre

INTRODUCTION

Visceral pain is the major complaint of patients with functional gastrointestinal disorders like irritable bowel syndrome (IBS) (1). Patients generally experience visceral hypersensitivity to normal physiological bowel movements in their distal colon and rectum (colorectum) in the absence of apparent structural gut damage or inflammation (2). Clinical studies indicate that sensitized primary afferents of the colorectum contribute to the persistent discomfort and pain characteristic of IBS (3–5). Using several preclinical rodent models of IBS, research by us and others previously documented the sensitization of both mechanosensitive and mechanically insensitive afferents innervating the colorectum that correlated with the development of behavioral colorectal hypersensitivity (2, 6–10). Notably, a single intracolonic instillation of 2,4,6-trinitrobenzenesulfonic acid (TNBS) induced overt colorectal inflammation, the recovery (over

Correspondence: B. Feng (fengb@uconn.edu).
Submitted 1 October 2020 / Revised 12 January 2021 / Accepted 27 January 2021

10–14 days) of which was accompanied with persistent afferent sensitization and behavioral colorectal hypersensitivity (11). The TNBS model recapitulates the symptoms of patients with postinfectious IBS (PI-IBS), i.e., development of persistent IBS symptoms after experiencing a bout of intestinal infection (12).

Visceral pain is usually evoked by mechanical stimuli to hollow visceral organs; other stimulus modalities like noxious tissue squeezing, cutting, heating, or even inflammation are generally insufficient to evoke perception from the viscera [see Ref. 13 for a recent review]. Thus, to further advance the understanding and treatment of visceral pain requires focused research on colorectal mechanotransduction, i.e., encoding the mechanical stress and strain on local tissue into trains of action potentials by sensory afferents in the colorectum. Neural encoding by colorectal afferents in response to mechanical stimuli in both naïve and visceral hypersensitive mice has been systematically studied by extracellular single-unit recordings from afferent axons [e.g., (6, 14–21)], and to a lesser degree by intracellular recordings from afferent somata in the dorsal root ganglion (DRG) (22, 23). In addition, our recent optical recording approach using genetically encoded calcium indicators GCaMP6f at intact DRG allowed high-throughput recordings of colorectal afferent neural activities (24). Those afferent neural activities are generated by the spike initiation process of mechanotransduction, which takes place at the microns-thick afferent axons embedded in the colorectal wall (18, 25), a focal region that is relatively understudied. Current knowledge about colorectal afferent fibers includes their anatomical locations and morphology in the colorectal wall, revealing that they are mostly free-nerve endings across different sublayers in the colorectum (26, 27). Knowledge is scarce regarding morphological changes of colorectal afferent fibers during development of IBS-like visceral hypersensitivity. Previously, apparent changes of neuronal fibers in the colorectum were detected in the intracolonic TNBS mouse model of PI-IBS using antibody staining against a pan-neuronal marker protein gene product 9.5 (PGP 9.5), which indicated apparent reduction of nerve fiber density following TNBS treatment with recovery 14 to 28 days posttreatment (11). However, it remains undetermined to what extent extrinsic afferent fibers change their morphology and density in the colorectum following TNBS treatment.

Most extrinsic afferents are glutamatergic neurons that express one of the three vesicular glutamate transporter (VGLUT) subtypes (28). Our prior study indicated that colorectal afferents predominantly express subtype 2 (VGLUT2); less than 10% of the colorectal DRG neurons express VGLUT1 or VGLUT3 (29). We also showed previously that channelrhodopsin2 tagged with fluorescent protein EYFP (ChR2-EYFP) was efficiently transported to afferent endings in the colorectum permitting functional characterizations (17, 25). In this study, we took advantage of the possibility to selectively tag VGLUT2-expressing colorectal primary afferent fibers to systematically analyze morphological changes following intracolonic TNBS instillation in Cre-LoxP transgenic mice, in which most afferent DRG neurons were tagged with ChR2-EYFP by the VGLUT2 promoter (VGLUT2-Cre) (30). We further confirmed that VGLUT2-Cre labeled only a small fraction of myenteric neurons (2.6%) and virtually no neural somata in autonomic ganglia, in contrast to efficient labeling (78%) of colorectal DRG neurons (24). We also conducted optical tissue clearing on whole mount colorectum by adapting a SeeDB protocol originally developed for clearing brain tissues (30), which allowed confocal imaging of nerve fibers through the thickness of the colorectal wall. We then conducted three-dimensional vector tracing of nerve fibers from the confocal image stacks for systematic quantification of nerve fiber location, density, and morphology before and after TNBS treatment.

MATERIALS AND METHODS

All experimental procedures were reviewed and approved by the University of Connecticut Institutional Animal Care and Use Committee (IACUC).

Transgenic Mice

Homozygous Ai32 mice (C57BL/6 background; strain no. 024109, The Jackson Laboratory, Connecticut) and homozygous VGLUT2-Cre mice (strain no. 28863, Jackson Laboratory, Connecticut) were crossbred. Ai32 mice carry the channelrhodopsin2 gene "ChR2(H134R)-EYFP" in the Gt (ROSA) 26Sor locus, which is preceded by a LoxP-flanked STOP cassette to prevent its expression. By crossing Ai32 mice with VGLUT2-Cre mice, the Cre-expressing cell population has the STOP cassette trimmed, resulting in expression of ChR2-EYFP in glutamatergic neurons expressing VGLUT2, which make up the vast majority of sensory neurons innervating the distal colon and rectum (colorectum) (29). Offspring of both sexes aged 8–14 wk heterozygous for VGLUT2-Cre and ChR2-EYFP genes (i.e., VGLUT2/ChR2) were used for the study.

To further confirm the expression efficiency of VGLUT2-Cre mice, we crossed VGLUT2-Cre mice with another reporter line, i.e., the tdTomato mice (Ai14, strain no. 7914, The Jackson Laboratory, Connecticut) as described previously (24). TdTomato filled the cytoplasmic space to allow easy quantification of DRG neurons. Offspring with heterozygous tdTomato (tdT) and VGLUT2-Cre genes (i.e., VGLUT2/tdT) were used for the study.

Mouse PI-IBS Model by Intracolonic TNBS Treatment

Mice were lightly anesthetized (isoflurane), and either saline or TNBS (0.2 mL @ 10 mg/mL in 50% ethanol; Sigma-Aldrich, St. Louis, MO) was administered transanally via a 22-gauge feeding needle with an oval-shaped tip of Ø1.25 mm (no. 8061-22, Fine Science Tools, Foster City, CA). Under anesthesia, mice were held in a head down position (~30°) for 5 min to ensure retention of TNBS in the colon. All mice receiving TNBS showed symptoms of diarrhea and detectable weight loss within 4 days of treatment. Dietary gel (NGB-1, Bio-Serv, Flemington, NJ) was provided to mice showing severe weight loss (>5% original body weight). Our prior study indicated significant loss of nerve fibers in the colorectum at *day 7* post-TNBS treatment and complete recovery by *day 28* (11). Accordingly, we designed the current study to assess nerve fiber density and morphology in VGLUT2/ChR2 mice at *days 7* and *28* post-TNBS.

Tissue Preparation for Whole Mount Optical Clearing

Seven or 28 days after intracolonic TNBS or saline, mice were deeply anesthetized (isoflurane) and euthanized by transcardiac perfusion from the left ventricle with ice-cold oxygenated Krebs solution (in mM: 117.9 NaCl, 4.7 KCl, 25 $NaHCO_3$, 1.3 NaH_2PO_4, 1.2 $MgSO_4$, 2.5 $CaCl_2$, and 11.1 D-glucose). The excised ~30 mm of distal colorectum was cannulated and distended to 20 mmHg with phosphate-buffered saline (PBS) using a custom-built distending device, an innocuous pressure that prevents folding of the colorectal wall (31). The colorectum was distended for 1 min, rested for 1 min, and distended/rested five times in total. After the distending protocol, the colorectum generally displayed a cylindrical shape as shown in Fig. 1*A*. The colorectum was then cut open along the mesentery and fixed with 4% (wt/vol) paraformaldehyde (PFA, Sigma-Aldrich, St. Louis, MO) dissolved in PBS at 4°C for 3 h.

Optical Clearing by Adapting the SeeDB Protocol

To optically clear the colorectum, we adopted the protocol published by Ke et al., which was originally developed for clearing mouse brain tissue (30). Briefly, the fixed samples were rinsed with PBS three times and then submerged in 20–30 mL of 20%, 40%, 60%, 80%, and 100% (wt/vol) fructose for 3 h, 3 h, 12 h, 12 h, and 24 h, respectively. Afterward, the samples were submerged in SeeDB solution (80.2% wt/wt fructose) for 24 h. The 20%–100% fructose solutions were prepared with diluted PBS (10 times dilution), and the SeeDB solution was prepared with deionized H_2O. The clearing process was conducted in a dark environment with sample tubes placed on a gentle shaker at room temperature. Samples were further incubated in refractive index matching solution (RIMS, see Ref. 30 for details) overnight at 4°C and divided longitudinally into three 10-mm-long segments (i.e., colonic, intermediate, and rectal regions, proximal to distal) as shown in Fig. 1*B*, according to our previous reports (32, 33). The anus was removed from the study. We mounted each segment in RIMS on glass slides and sealed the coverslip with nail polish. Incubating and mounting samples in RIMS with a refractive index (RI) of ~1.47 enhanced the optical clarity by reducing the mismatch of RIs between the processed sample and the glass microscope objective (34).

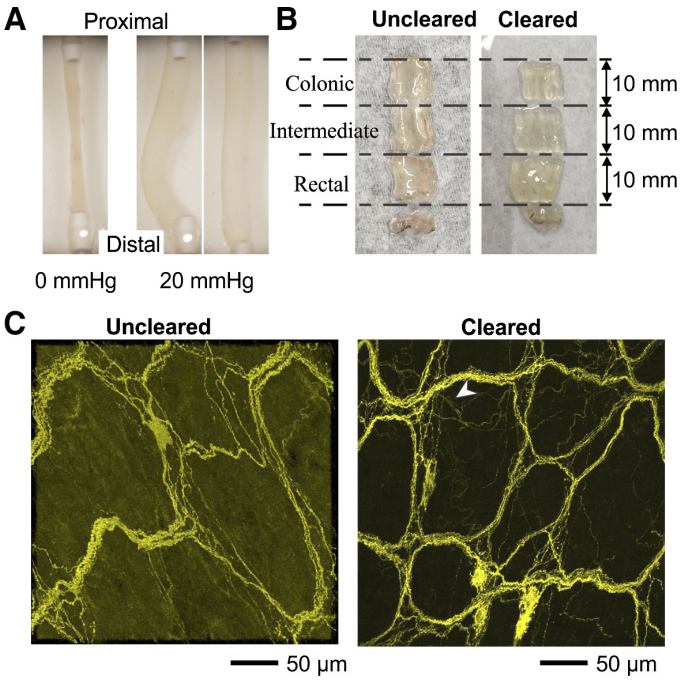

Figure 1. Optical clearing of mouse colorectum for through-thickness imaging. *A*: distal mouse colorectums were cannulated, distended to 20 mmHg, fixed by 4% paraformaldehyde. *B*: bright-field images of uncleared versus optically cleared colorectum. The distal 30 mm of the colorectum was evenly divided into colonic, intermediate, and rectal segments (from proximal to distal). The anus was removed from the study. *C*: confocal fluorescent images of VGLUT2-positive nerve fibers captured from uncleared colorectum, in comparison with images from optically cleared colorectum. Fine fibers were observed in images from cleared colorectum as indicated by the white arrowhead. VGLUT2, vesicular glutamate transporter type 2.

Whole Mount Immunostaining of the Colorectum

To quantitatively determine the expression efficiency of the VGLUT2-Cre mice, we conducted immunostaining on whole-mount colorectum harvested from both VGLUT2/ChR2 and VGLUT2/tdT mice. Mice were euthanized via isoflurane inhalation and perfused with a calcium-free Krebs solution containing 10 mM EDTA and 1 μM nifedipine (Sigma-Aldrich, St. Louis, MO). Distal colons were harvested and distended using the same distending protocol as described in *Tissue Preparation for Whole Mount Optical Clearing*. Inflated colons were fixed in the tubular shape in 4% PFA at 4°C for 30 min. The fixed tissues were washed in PBS with 0.1% Triton X-100 (Sigma-Aldrich) and then incubated in blocking solution containing 4% donkey serum, 0.4% Triton X-100, and 1% bovine serum in PBS for 45 min (35). To visualize neural somata, the tissues were incubated with a mouse biotin-conjugated monoclonal antibody against HuC/HuD (1:200, Fisher Scientific, East Greenwich, RI) for 48 h at 4°C, and then were incubated in Streptavidin conjugated with Alexa Fluor 594 (1:200, Jackson ImmunoResearch, West Grove, PA) for 2 h at room temperature. The colorectum was then flattened, mounted whole on diamond white glass slides serosal side up (Globe Scientific, Inc., Mahwah, NJ), covered by thin glass slips (Corning, Inc., Corning, NY), and imaged at the myenteric plexus using a confocal microscope (A1R, Nikon Inc., Melville, NY).

Immunohistochemistry

VGLUT2/ChR2 mice were euthanized via isoflurane inhalation. The autonomic ganglions, e.g., major pelvic ganglion (MPG) and lumbar sympathetic chain (LSC), were dissected out and fixed with 4% (wt/vol) paraformaldehyde dissolved in PBS for 2 h at room temperature. After cryoprotection in 20% sucrose, fixed tissues were embedded in OCT compound (Sakura Finetek, Tokyo, Japan), frozen at −20°C, and sectioned at 20 μm. Tissue sections were incubated in a rabbit antibody against tyrosine hydroxylase (1:400, MilliporeSigma, St. Louis, MO), and the signals were further amplified by Alexa Fluor 594-conjugated antirabbit IgG (1:400, Abcam, Cambridge, MA).

Imaging throughout Colorectal Wall under Confocal Microscope

Cleared colorectal samples were mounted serosal side up in RIMS on diamond white glass slides and covered by thin

glass slips. The colorectal wall (thickness from 100 to 300 μm) was scanned from serosa to mucosa with a Nikon A1R spectral confocal microscope (Nikon Inc., Melville, NY) using a ×40 Plan Fluor Oil immersion objective (working distance 240 μm, NA 1.30). To capture fine structures of unmyelinated nerve axons (~1 μm thick according to Ref. 27), we scanned the sample in 0.3-μm steps at 1,024 × 1,024 pixel resolution either through the wall thickness or up to 200 μm, limited by the working distance of the ×40 objective. We implemented intensity correction in the *Z* (through-thickness) axis to increase scanning laser power for deep tissues. We acquired images by setting the parameters in the Nikon NIS-Elements software suite that came with the microscope. In each sample, two image stacks were recorded at random spots. To avoid confounding factors, areas with large blood vessels that showed strong autofluorescence were not imaged.

Vector Path Tracing of VGLUT2-Positive Nerve Fibers from Image Stacks

The three-dimensional volume from confocal image stacks through the colorectal wall was divided into subvolumes following the anatomical separation of longitudinal muscular, myenteric plexus, circular muscular, submucosal, and mucosal layers. Data analysists were blinded to the TNBS or saline treatment to the mice. In each subvolume except the myenteric plexus, VGLUT2-positive nerve fibers were traced using a semiautomated neurotracing plugin in ImageJ software (v. 1.8.0; National Institutes of Health, Bethesda, MD), i.e., "Simple Neurite Tracer" (36). This approach permitted the creation of vector paths of individual nerve fibers, including fibers with a curvy appearance by approximating with infinitesimal linear segments. The traced vector paths were extracted as "*x*," "*y*," and "*z*" coordinates at the ends of the full path as well as their lengths to allow post hoc statistical analyses of nerve fibers. Vector path tracing was not performed in the myenteric plexus, where nerve fibers clustered into thick bundles, which prevented definitive tracing of individual fibers.

Quantification of VGLUT2-Positive Nerve Fibers

Nerve fiber density quantified as length per volume. After vector path tracing, the density of VGLUT2-positive nerve fibers in the longitudinal muscular, circular muscular, submucosal, and mucosal layers was calculated as total nerve fiber length divided by tissue volume. The total fiber length in each tissue volume was acquired by summing up all traced vector paths within the volume.

Nerve fiber density quantified as percentage of fluorescent signals. Particularly in the myenteric plexus, VGLUT2-positive nerve fibers organized into thick bundles that weaved into a mesh-like network, making it impossible to trace individual nerve fibers within. In such cases, we proceeded with the quantification of the density of VGLUT2-positive nerve tissue as the area percentage of fluorescent signals within the myenteric plexus. Detection of the fluorescent signal threshold was reported previously (24). Using ImageJ, we projected each image stack from the myenteric plexus with "maximum intensity *z*-projection" to convert into an 8-bit grayscale image. The threshold was set to exclude at least 99.99% of the background intensity based on its Gaussian distribution. The threshold value was calculated from the standard normal distribution (Z) equation: threshold = 3.72 SD + M, where 3.72 was the *Z*-score at $P = 0.9999$, SD and M were the standard deviation and mean of background intensities in 8-bit grayscale (0–255), respectively. The percentage of fluorescent signals was calculated as the area ratio above the threshold in the 8-bit grayscale image.

Fiber ending curviness quantified by the linearity index. The distal afferent endings (50 to 300 μm) in the colorectum are putative transducer zones for encoding external stimuli into trains of action potentials. Most distal VGLUT2-positive nerve fibers in the submucosa appear curvy and "meandering," in contrast to fibers in muscular or mucosal layers that are generally aligned with the muscle bundles or the crypts. From vector path tracing, we defined the linearity index (*LnIdx*) of individual nerve endings as the ratio between the path length of the distal 50–300-μm axon and the direct distance between the two ends of the distal axon.

$$LnIdx = \frac{L}{\sqrt{(x_2 - x_1)^2 + (y_2 - y_1)^2 + (z_2 - z_1)^2}}$$

where L is the length of the distal nerve axon, and (x_1, y_1, z_1) and (x_2, y_2, z_2) are coordinates of the two ends. The linearity index *LnIdx* is 1 for an ideally straight nerve fibers, and greater than 1 for curvy and meandering fibers. For unmyelinated free nerve endings, the exact distribution of transducer molecules for mechanical stimuli remains undetermined but are generally presumed to be expressed in the distal ~100 microns of the endings, i.e., the presumed transducer zone (18). When determining the *LnIdx*, we analyzed the distal 50–300 μm of the nerve endings in the colorectum, which likely encompass the transducer zone of the fibers.

Data Analysis

Data are presented as means ± SD. Error bars in bar graphs of the figures indicate SD. One-way and two-way analyses of variance (ANOVA) were used to test the differences between control and treated groups. Bonferroni post hoc multiple comparison was performed if difference is significant. The normality of data was assessed by Shapiro–Wilk test. Differences were considered significant when $P < 0.05$. Statistical analysis was performed using SigmaStat v. 4.0 (Systat Software, San Jose, CA).

RESULTS

Optical Clearing of Mouse Colorectum for Whole Mount Imaging

As shown in Fig. 1*A*, the colorectum was distended by 20 mmHg pressure to prevent wall folding following the protocol described in the MATERIALS AND METHODS. The cylindrical colorectum was cut open, fixed by PFA, optically cleared following the modified SeeDB protocol, and divided longitudinally into three segments: colonic, intermediate, and rectal segments. As displayed in bright-field photographs in Fig. 1*B*,

cleared colorectum showed more glass-like transparency than the uncleared counterpart. Displayed in Fig. 1*C* are examples of *Z*-stack confocal microscope images of the same thickness (78 μm) from uncleared and cleared colorectal walls of VGLUT2/ChR2 mice. Thick nerve bundles in the myenteric plexus were able to be captured in the uncleared colorectum, but individual microns-thick fibers were only visible in the cleared colorectum (marked by the white arrowhead) and obscured in the uncleared colorectum. This is likely due to the dramatically reduced laser power for imaging the cleared tissue than for the uncleared, yielding significantly lower background signals to enhance the detection of fine nerve fibers.

Validation of VGLUT2 Expression in Colorectal Nerve Innervations

To validate the expression efficiency of VGLUT2-Cre, we not only cross bred VGLUT2-Cre gene line mice with the floxed channelrhodopsin2 (ChR2) reporter line, but also a tdTomato (tdT) reporter line. Displayed in Fig. 2, *A* and *B*, are confocal images from cleared colorectum harvested from VGLUT2/tdT and VGLUT2/ChR2 mice, respectively. Both reporter lines revealed comparable VGLUT2-positive neural tissue patterns in the myenteric plexus, i.e., the mesh-like thick nerve bundles connecting myenteric ganglia. However, the tdT reporter was inferior at labeling individual fine fibers in the submucosal layer as compared with the ChR2 reporter (Fig. 2*C*). Both tdT and ChR2 reporter lines were efficient in labeling the cell somata in the myenteric ganglia as indicated by arrowheads in Fig. 2, *A* and *B*. Thus, we used both reporter lines to quantify the proportions of positive neurons in the myenteric plexus and exclusively used the VGLUT2/ChR2 mice for quantification of nerve axons in the colorectum.

In our previous study using the tdT reporter line, we reported that VGLUT2-Cre induced expression in 78% of colorectal afferent neurons in the DRG (24). To assess the expression efficiency in the enteric nervous system, we marked the neural somata with anti-Hu antibody as shown in Fig. 2*D*. From five through-thickness image stacks taken from five different colorectums (one from each colorectum), we identified 266 neurons in myenteric plexus immunoreactive to anti-Hu, seven of which were also VGLUT2 positive. This indicated that VGLUT2-Cre only induced expression in a very small fraction of myenteric neurons (2.62 ± 1.88%). Throughout the myenteric plexus, we did not find any VGLUT2-positive neural somata that had negative anti-Hu immunoreactivity. We did not observe any VGLUT2-positive somata in the submucosal plexus (data not shown), consistent with prior antibody-based immunostaining results (29).

Besides sensory afferent and enteric innervations, the colorectum is also innervated by autonomic neurons, mostly postganglionic sympathetic neurons in the lumbar sympathetic chain (LSC) and the major pelvic ganglion (MPG) (37). We thus harvested LSC and MPG from VGLUT2/ChR2 mice both 12 days post-TNBS and saline treatment and stained the tissue sections with an antibody against tyrosine hydroxylase (TH), a marker for sympathetic neurons. As shown in Fig. 3*A*, VGLUT2-Cre did not label any somata in the MPG of mice receiving TNBS, which contained TH-immunoreactive

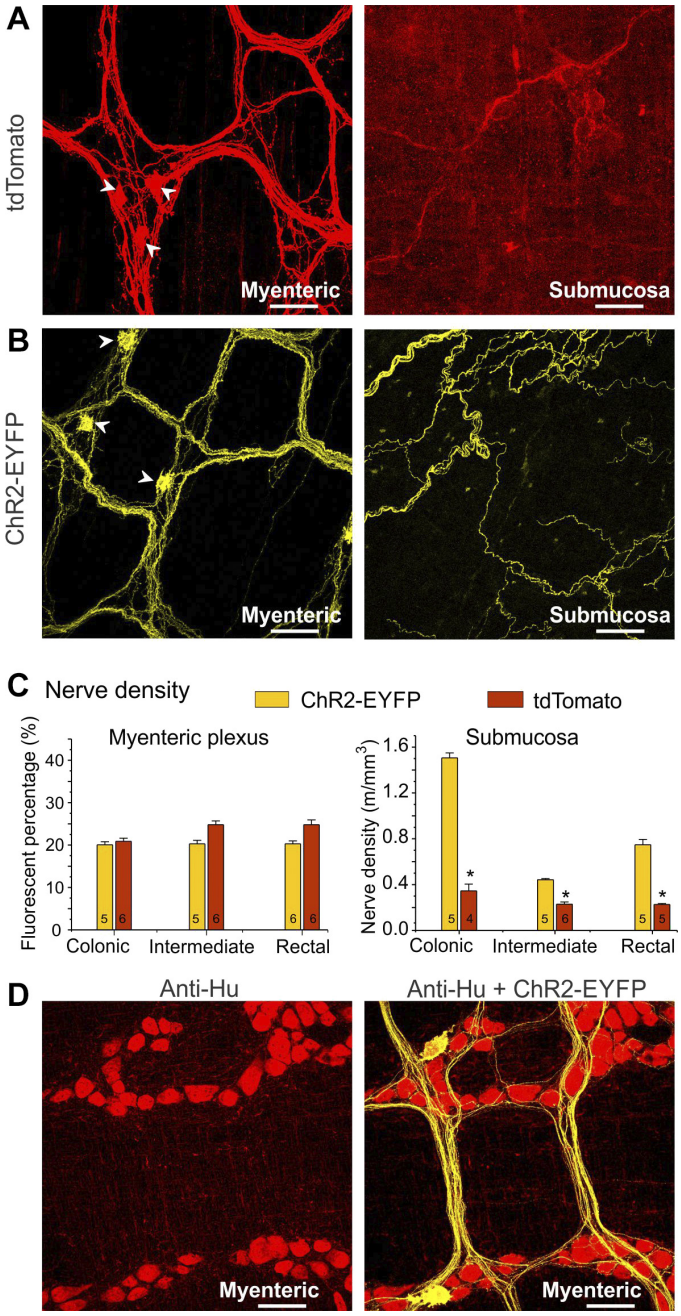

Figure 2. Validation of VGLUT2 expression in colorectal nerve innervations. In optically cleared colorectum, VGLUT2-positive signals were visualized using a tdTomato reporter (*A*) and a channelrhodopsin2-EYFP reporter (*B*). *C*: comparison of colorectal nerve density between VGLUT2/ChR2 and VGLUT2/tdT mice in myenteric plexus and submucosa layers. The data are shown as means ± SE. Sample numbers are shown in each column. *D*: VGLUT2-Cre only stained a very small fraction (2.62%) of neurons in the myenteric plexus, the somata of which were marked in red by anti-Hu antibody. Scale bars: 50 μm. *$P < 0.05$. ChR2, channelrhodopsin2; VGLUT2, vesicular glutamate transporter type 2.

sympathetic fibers and somata. Similarly, the TH-positive autonomic fibers and somata did not colocalize with VGLUT2-positive fibers in the LSC from TNBS-treated mice (Fig. 3*B*). Also, no colocalization between VGLUT2-positive and TH-positive fibers or somata was detected in MPG from saline-treated mice (Fig. 3*C*), consistent with a previous

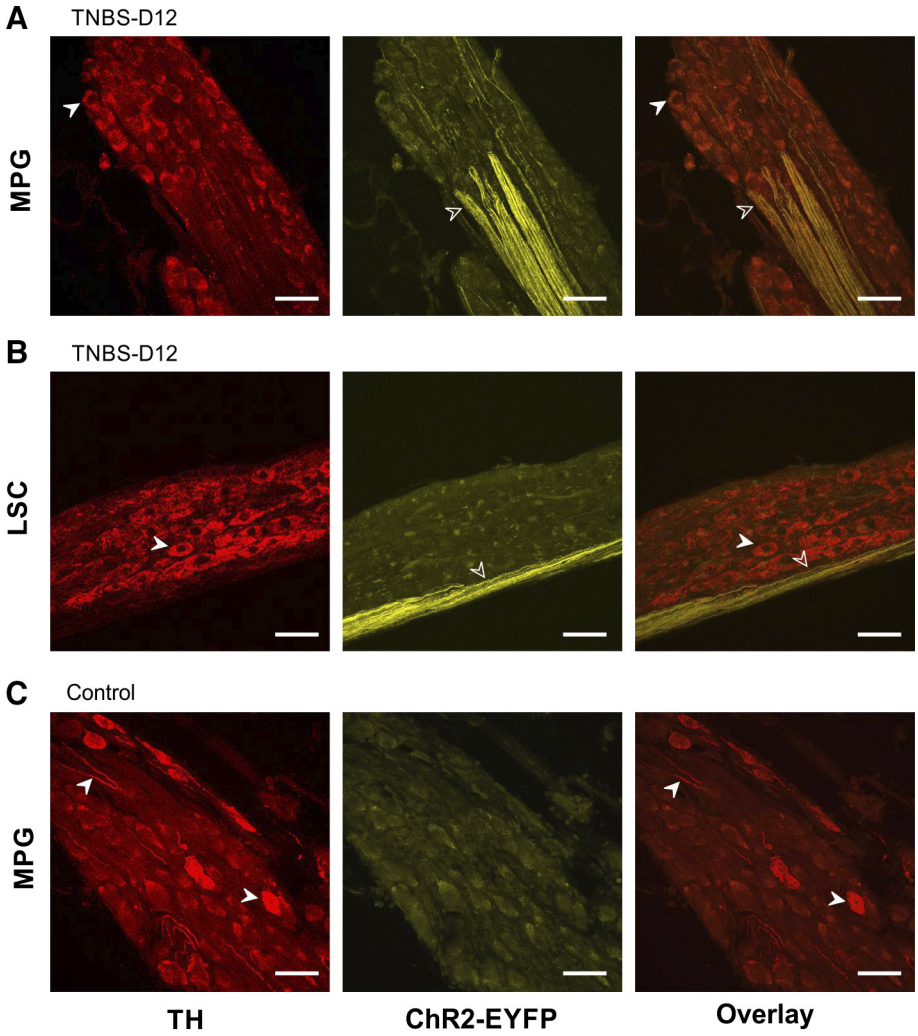

Figure 3. Absence of VGLUT2 expression in autonomic ganglia, i.e., the major pelvic ganglion (MPG) and lumbar sympathetic chain (LSC). Sympathetic neurons and fibers marked by an antibody against tyrosine hydroxylase (TH) are indicated by solid arrowheads, which do not overlap with ChR2-EYFP fibers (driven by VGLUT2-Cre) as indicated by open arrowheads. Expression of VGLUT2 was not identified in TH-positive autonomic neurons in either MPG (*A*) or LSC (*B*) harvested 12 days post-TNBS, nor was in MPG harvested from saline-treated controls (*C*). Scale bars: 50 μm. TH, tyrosine hydroxylase; TNBS, 2,4,6-trinitrobenzenesulfonic acid; VGLUT2, vesicular glutamate transporter type 2.

report (37). These above results collectively indicate that EYFP-labeled nerve fibers in the VGLUT2/ChR2 colorectum consist of mostly extrinsic sensory afferents and a very small fraction of intrinsic myenteric fibers.

Through-Thickness Imaging of VGLUT2-Positive Fibers in the Colorectum

Image stacks of VGLUT2-positive fibers in cleared colorectum were taken via confocal microscopy at 0.3-μm steps through the wall thickness from serosal to mucosal surfaces, or up to 200 μm (limited by the working distance of the ×40 objective). Wall thickness of the distal colorectum increased progressively from ~120 μm in the colonic region to over 250 μm in the rectal region, as previously reported (31, 38); most of the thickness was attributable to the mucosal layer. Thus, confocal imaging captures the entire wall thickness in the colonic and intermediate segments, but only a portion of the mucosal layer in the rectal segment. Shown in Fig. 4 are typical *Z*-stack images at five anatomically distinct layers of the colorectum: mucosal (M), submucosal (SM), circular muscular (CM), myenteric plexus (MP), and serosal and longitudinal muscular (S-LM) layers. VGLUT2-positive nerve fibers were abundant in submucosal and myenteric plexus layers, which coincide with regions of the two enteric plexuses in the colorectum. VGLUT2-positive nerve fibers were also widely present around the crypts in the mucosal layer and present to a lesser degree in circular muscular layers. We did not detect any nerve fibers that were definitively embedded in the muscle bundles in the longitudinal muscular layer. Also, no VGLUT2-positive fibers were detected in the serosal layer. Typical images of VGLUT2-positive fibers in colorectums harvested at *day 7* and *28* post-TNBS treatment (TNBS-D7, TNBS-D28) are also displayed in Fig. 4. In colorectums harvested on *day 7* post-TNBS, we detected an apparent reduction of VGLUT2-positive nerve fibers, particularly evident in the mucosal and submucosal areas (white arrowheads). In colorectums harvested on *day 28* post-TNBS, there was no apparent reduction in VGLUT2-positive nerve fibers in any layer.

Density of VGLUT2-Positive Nerve Fibers in the Colorectum

We quantified the density of nerve fibers in the myenteric plexus by calculating the area fraction of VGLUT2-positive fluorescent signals within the total area. Displayed in Fig. 5*A* is a representative image stack of a 25-μm-thick myenteric

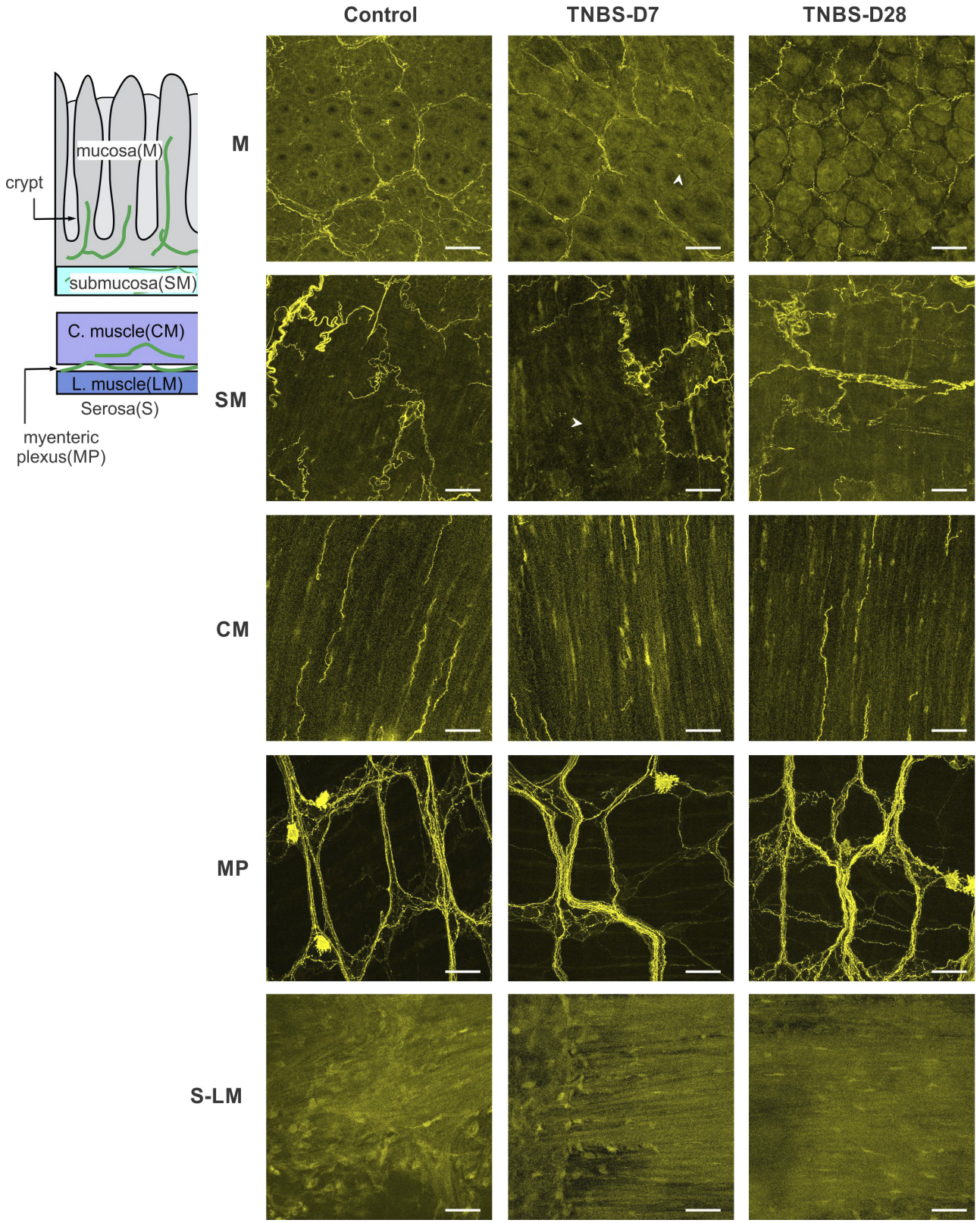

Figure 4. Representative through-thickness imaging of VGLUT2-positive fibers in the colorectum. Confocal images were taken from colorectums harvested from control and TNBS-treated mice at *day 7* (TNBS-D7) and *day 28* (TNBS-D28). CM, circular muscular layer; M, mucosa; MP, myenteric plexus; S-LM, serosal and longitudinal muscular layer; SM, submucosa; TNBS, 2,4,6-trinitrobenzenesulfonic acid; VGLUT2, vesicular glutamate transporter type 2. Scale bars: 50 μm.

AJP-Gastrointest Liver Physiol • doi:10.1152/ajpgi.00363.2020 • www.ajpgi.org

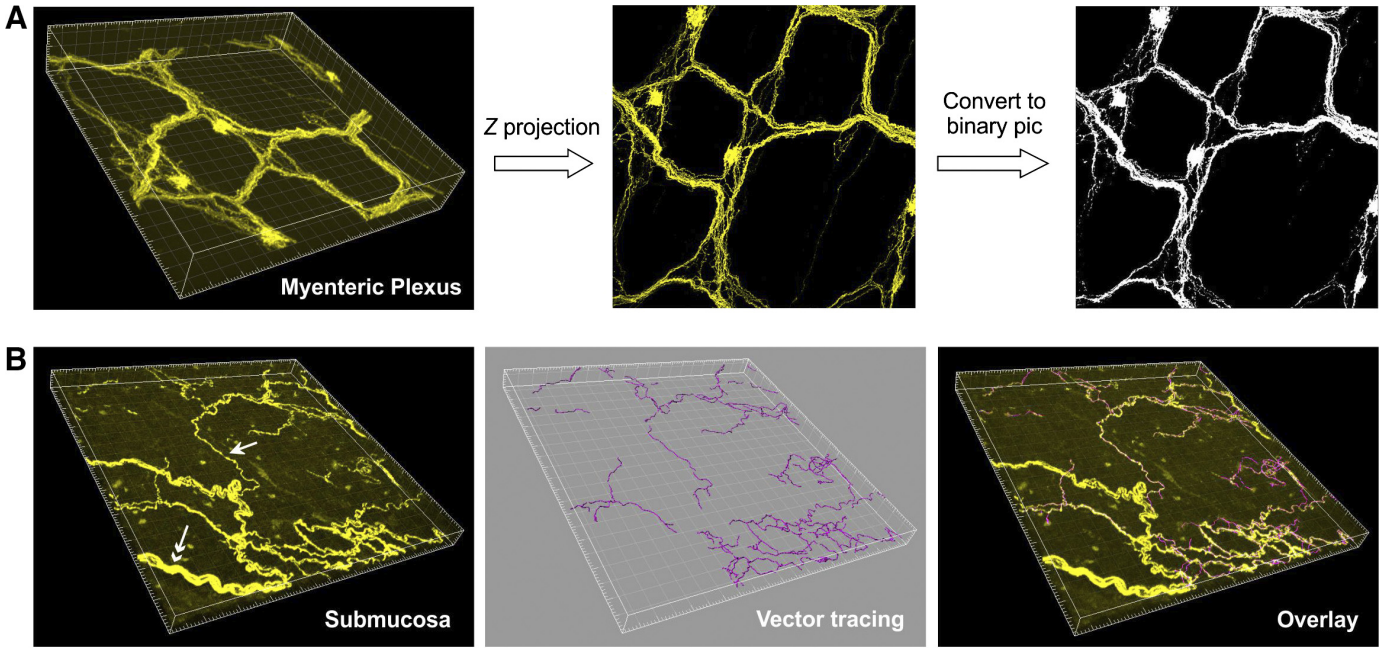

Figure 5. Quantification of the density of VGLUT2-positive nerve fibers in the colorectum. *A*: the density of VGLUT2-positive neural signals in the myenteric plexus was quantified by the area fraction of positive fluorescent signals after flattening the confocal image stacks. *B*: the density of VGLUT2-positive fibers (e.g., indicated by white arrow) in other layers of the colorectum was quantified by the nerve length per volume. For consistency, nerve bundles containing more than one axon (e.g., indicated by white double arrow) were excluded from the analysis. Vector path tracing was conducted on individual nerve fibers as indicated by the pink traces. VGLUT2, vesicular glutamate transporter type 2.

plexus, which was transformed into an 8-bit *Z*-stack image (intensity from 0 to 255) and further converted into a binary image by setting a detection threshold based on the mean (3.619) and standard deviation (1.379) of the background intensity. The fraction of VGLUT2-positive nerve fibers in the myenteric plexus area was determined by dividing the mean intensity of the binary image 58.01 by 255, i.e., 22.75%. In contrast, fiber density in muscularis, submucosa, and mucosa was quantified by vector path tracing using the "simple neurite tracer" plug-in in ImageJ. As shown in a typical example in Fig. 5*B*, individual nerve fibers (marked by arrow) and thick nerve bundles consisting of many axons (marked by double arrow) were both present in the tissue. For consistent analyses, we only quantified individual fibers and did not include nerve bundles. The total length of individual nerve fibers in Fig. 5*B* was 4,036 μm in a volume of 2.18×10^6 ($322.18 \times 322.18 \times 21$) μm^3, resulting in a fiber density of 1.85 m/mm^3.

As summarized in Fig. 6, the density of VGLUT2-positive fibers was determined at random locations in the colonic, intermediate, and rectal segments of five colorectums harvested from control VGLUT2/ChR2 mice receiving intracolonic saline treatment. VGLUT2-positive nerve density in the myenteric plexus (MP), circular muscular (CM), and mucosal (M) layers was comparable in all three longitudinal segments (one-way ANOVA, $F = 0.54$, $P = 0.60$ for MP; $F = 0.007$, $P = 0.99$ for CM; $F = 0.37$, $P = 0.70$ for M). In contrast, nerve fiber density in the submucosal (SM) layer was significantly greater in the colonic segment than in the two distal segments (one-way ANOVA, $F = 43.29$, $P < 0.001$; post hoc analyses, $P < 0.01$ for colonic vs. rectal and colonic vs. intermediate). VGLUT2-positive nerve fibers were absent in the serosal and longitudinal muscular (S-LM) layers in all three longitudinal segments. In colonic segments, nerve fiber density in the CM layer was significantly lower than in the SM and M layers ($F = 12.65$, $P < 0.01$; post hoc analyses, $P < 0.001$ for CM vs. SM, $P < 0.05$ for CM vs. M). In intermediate segments, the fiber density in the CM and SM layers were comparable but significantly less than in the M layer ($F = 21.22$, $P < 0.001$; post hoc analyses, $P < 0.001$ for M vs. CM, $P < 0.001$ for M vs. SM). In rectal segments, the fiber density in the CM layer was less

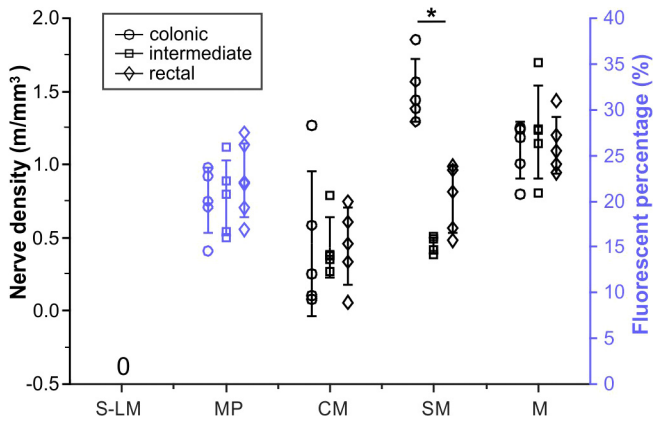

Figure 6. VGLUT2-positive nerve fiber densities quantified as nerve length per unit volume in serosal and longitudinal muscular (S-LM), circular muscular (CM), submucosal (SM), and mucosal (M) layers. As indicated with blue markers, neural tissue density in the myenteric plexus (MP) was quantified as the area fraction of positive fluorescent signals shown in the right *y* axis. The circle, square, and diamond markers indicate nerve density in colonic, intermediate, and rectal segments, respectively. *$P < 0.05$. VGLUT2, vesicular glutamate transporter type 2.

than in the M layer but comparable with the SM layer (F = 11.28, $P < 0.01$; post hoc analyses, P = 0.001 for CM vs. M, P = 0.07 for CM vs. SM). Overall, nerve fiber density is lowest in the CM layer in all three segments.

Loss (*Day 7*) and Recovery (*Day 28*) of VGLUT2-Positive Nerve Fiber Density following Intracolonic TNBS Treatment

Using through-thickness confocal imaging and fiber quantification, we determined the change in nerve fiber density on *day 7* after intracolonic saline treatment (control) and *days 7* and *28* after intracolonic TNBS treatment (TNBS-D7, TNBS-D28) and summarized the results in Fig. 7. Colorectums were harvested from five control, 10 TNBS-D7, and eight TNBS-D28 mice. As shown in Fig. 7*A*, nerve fiber density in CM layers was unaffected by TNBS treatment in all three longitudinal segments [two-way ANOVA, $F_{2,35}$ = 0.98, P = 0.39 for segments; $F_{2,35}$ = 1.41, P = 0.26 for treatment]. In contrast, nerve fiber density in the TNBS-D7 group was significantly reduced in MP (Fig. 7*B*), SM (Fig. 7*C*), and M (Fig. 7*D*) layers in all three longitudinal segments [two-way ANOVA, $F_{1,8}$ = 50.16, $P <$ 0.001 for colonic SM; $F_{1,8}$ = 27.20, $P < 0.001$ for intermediate SM; $F_{1,8}$ = 11.04, $P < 0.05$ for rectal SM; $F_{1,9}$ = 13.11, $P < 0.01$ for colonic MP; $F_{1,9}$ = 8.13, $P < 0.05$ for intermediate MP; $F_{1,10}$ = 18.51, $P < 0.01$ for rectal MP; $F_{1,8}$ = 27.89, $P < 0.001$ for colonic M; $F_{1,8}$ = 15.12, $P < 0.01$ for intermediate M; $F_{1,7}$ = 19.80, $P < 0.01$ for rectal M]. In the TNBS-D28 group, nerve fiber densities completely recovered to control densities in most areas of SM, MP, and M layers (post hoc comparison, P = 0.81 for intermediate SM, P = 0.09 for rectal SM, P = 0.17 for colonic MP, P = 0.22 for intermediate MP, P = 0.43 for rectal MP, and P = 0.69 for rectal M, all vs. control). In some areas, nerve density did not fully recover at *day 28* post-TNBS, including in colonic SM (P = 0.003), colonic M (P = 0.11), and intermediate M (P = 0.16).

TNBS Impact on the Curviness (Quantified by Linearity Index) of Nerve Fibers within the Submucosa

Unlike the VGLUT2-positive nerve fibers in other layers of the colorectum that were generally aligned with the basal tissues (e.g., along the circular muscle bundles or around the crypts), fibers in the submucosa did not seem to follow any patterns but were significantly more meandering and curvy. Accordingly, we quantified the linearity index (*LnIdx*) in all distal 50- to 300-μm endings of the nerve axons in the submucosa following the description in the MATERIALS AND METHODS. We analyzed the *LnIdx* of a total 1,148 VGLUT2-positive fibers from five control, 10 TNBS-D7, and eight TNBS-D28 colorectums. Among the 1,148 fibers, 1,127 (98.2%) exhibited *LnIdx* graded arbitrarily but based on the range as low (1–1.67), medium (1.68–2.33), and high (2.34–3), which correspond to moderate, pronounced, and extreme curviness, respectively. Displayed in Fig. 8*A* are typical examples of fibers from these three groups. As shown in Fig. 8*B*, in control mice, most of the fibers identified across the different areas analyzed (>84%) exhibited moderate curviness, followed by fibers with pronounced curviness varying from 9.90% to 15.98%; the proportion of fibers exhibiting extreme curviness was not significant in any group (<4.3%) and received no further analysis. In mice undergoing TNBS

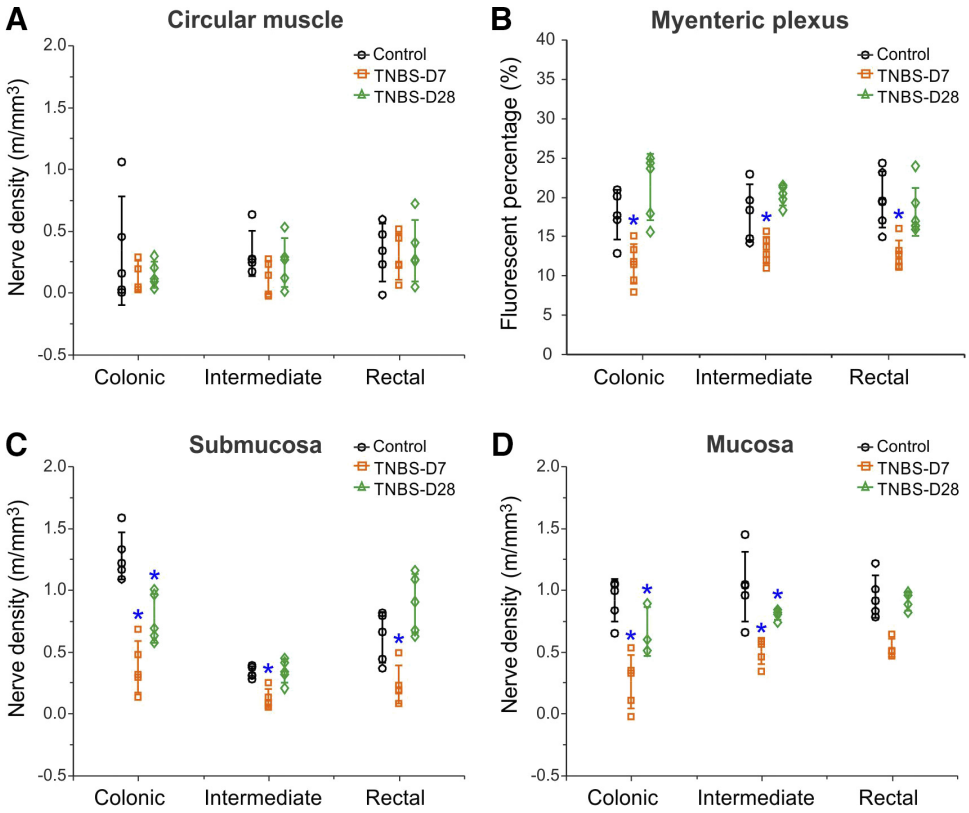

Figure 7. Altered VGLUT2-positive neural fiber densities in all layers of the colorectum following intracolonic TNBS treatment. The neural densities in control (black circle) and TNBS-treated colorectums at *day 7* (orange square) and *day 28* (green diamond) were quantified in circular muscular (*A*), myenteric plexus (*B*), submucosal (*C*), and mucosal layers (*D*). *Significant difference from control. TNBS, 2,4,6-trinitrobenzenesulfonic acid; VGLUT2, vesicular glutamate transporter type 2.

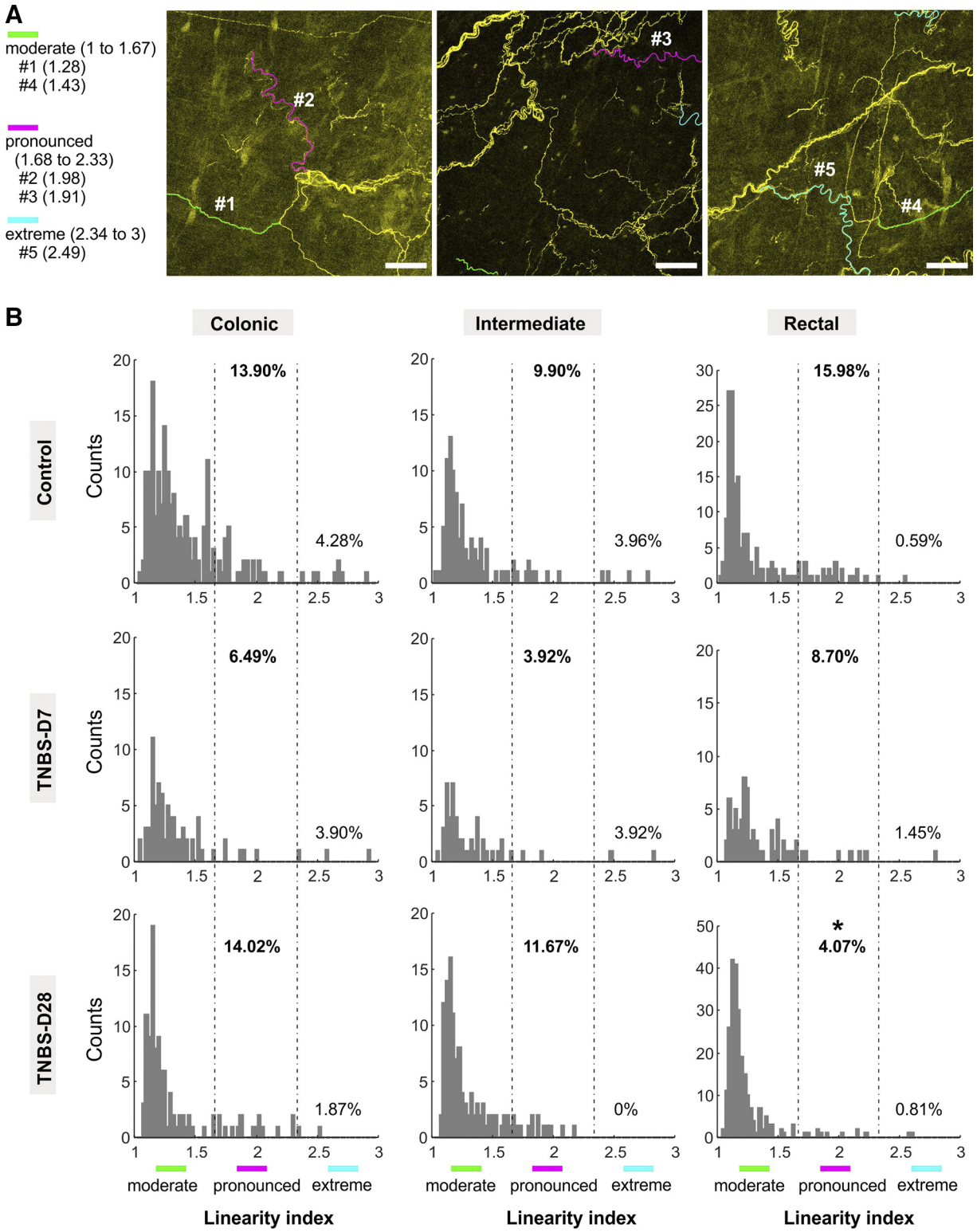

Figure 8. Quantification of the curviness by linearity index (*LnIdx*) of the distal 50–300-μm endings of the nerve axons in the submucosa following intracolonic TNBS treatment. *A*: typical submucosal nerve fibers with different levels of curviness, i.e., moderate (1–1.67, green), pronounced (1.67–2.33, magenta), and extreme (2.33–3, cyan). Scale bars: 50 μm. *B*: the *LnIdx* histograms of 1,127 fibers ranging from 1 to 3 (21 fibers with *LnIdx* beyond 3 were excluded). $*P < 0.05$. TNBS, 2,4,6-trinitrobenzenesulfonic acid.

treatment, fibers moderately curvy remained mostly unaffected in either proportion or *LnIdx*. The proportion of pronounced curvy fibers varied from 9.9% to 15.98% across different groups. In the TNBS-D7 group, the proportion of pronounced curvy fibers trended toward a reduction compared with control in all three longitudinal segments despite reaching no statistical significance (Fisher's exact test, P = 0.096 for colonic, P = 0.338 for intermediate, P = 0.213 for rectal vs. control). In the TNBS-D28 group, the proportion of pronounced curvy fibers was comparable with control at the colonic and intermediate segments (14.02%, P = 1.000 for colonic; 11.67%, P = 0.830 for intermediate vs. control) but was significantly lower than control level in the rectal segment (4.07%, $P < 0.001$). Pooling the *LnIdx* from all three segments, there was no statistical difference between the average *LnIdx* in control, TNBS-D7, and TNBS-D28 groups, which were 1.47 (n = 472), 1.42 (n = 202), and 1.31 (n = 474), respectively.

DISCUSSION

The principal innovation of the current study is the macro-level approach to quantify the morphology and density of overall VGLUT2-positive fiber innervations in the colorectum, which consist of mostly extrinsic sensory afferents. A handful of previous studies of colorectal afferent fibers focused on sparse neural tracing of a small number of fibers in the colorectum. For example, anterograde tracing from fine split filaments of spinal nerves revealed the presence of nerve fibers in all layers of the colorectum except the serosa (39–41). Tracing the pelvic nerve with an anterograde dye may unavoidably label nonafferents as evidenced by occasional staining of the somata of viscerofugal and major pelvic ganglion neurons (40). Recently, Spencer et al. (27) pioneered a novel tracing approach to exclusively label extrinsic afferents by sparse labeling of lumbosacral dorsal root ganglion.

In the current study, we took advantage of our recently reported method for genetic labeling of VGLUT2-expressing DRG neurons by use of a VGLUT2-Cre line to drive the expression of LoxP reporter genes, which labels ~80% colorectal afferent neurons to allow studying their nerve fiber patterns in the colorectum. Importantly, VGLUT2 has been found in ~97% and ~98% of colorectal afferent neurons present in lumbosacral (L6-S2) and thoracolumbar (T8-L1) DRGs, respectively (29). We also confirmed that VGLUT2-Cre did not drive any expression in neurons in autonomic ganglia, i.e., the MPG and LSC, which was consistent with a prior report on naïve mice (37). The same study also reported that axotomy, a severe peripheral nerve injury, led to sporadic VGLUT2-positive somata in the autonomic ganglia. In contrast, intracolonic TNBS enema in the current study was a much milder injurious stimulus and did not drive any detectable expression of ChR2-EYFP in the somata of autonomic ganglia in VGLUT2/ChR2 mice.

Here, we not only show a profuse distribution of VGLUT2-expressing fibers in the colorectal walls, we also reveal sporadic presence of VGLUT2-Cre-labeled neural somata in the myenteric plexus, contributing only ~2.6% of all neurons in the myenteric ganglia, and virtual absence of labeled somata in the submucosal plexus. This is consistent with our prior results on anterograde tracing of the pelvic nerve, and with the detection of a small number of myenteric plexus neurons expressing VGLUT2 transcript and protein (29). Collectively, the above reveals that most nerve fibers labeled by VGLUT2-Cre in the colorectum must be extrinsic sensory afferents. We previously used Advillin-Cre to drive the expression of channelrhodopsin2 in colorectal afferents, allowing optogenetic activation of colorectal afferent endings (17, 25). However, Advillin-Cre mice, especially females, have weak Cre expression in their oocytes and may drive nonselective expression beyond sensory afferents (breeding consideration for #032536, Jackson Laboratory, Farmington, CT). Similar to VGLUT2-Cre, CGRP-α or TrpV1 promoters were recently used to fluorescently label extrinsic colorectal afferents (42, 43). Unlike the VGLUT2-Cre, the CGRP-α and TrpV1 promoters are more selective to extrinsic sensory afferents, with no apparent staining of neural somata in the enteric plexuses. However, VGLUT2 appears to be more widely expressed in colorectal DRG neurons (97%–98%) than CGRP (57%–80%) or TrpV1 (64%–84%) from immune-staining studies of DRG sections (29, 44). Thus, VGLUT2-Cre potentially provides a more unbiased labeling of colorectal afferent neurons.

To label afferent fibers in the colorectum, here we tested two reporter fluorescent proteins and found strikingly different efficiencies at labeling fine neural structures in the colorectum: channelrhodopsin2-EYFP (ChR2) were transported from the cytosol in DRG somata to fine afferent axons in the colorectum, whereas tdTomato (tdT) filled the somata but did not label fine afferent axons, particularly in submucosa. This is likely due to the distance from DRG somata to afferent endings in the colorectum and the small axonal diameters of colorectal afferents; most colorectal afferents are slowly conducting C-fibers with axon diameters ~1 μm (15, 27). In our previous optogenetic studies, the transport of ChR2 to colorectal nerve terminals was evidenced by tonic excitation of colorectal afferents via focused blue light stimulation at endings in the colorectum (17, 25). Similarly, CGRP-α fused with the fluorescent reporter mCherry was reported to successfully label nerve axons in the colorectum (22, 43), likely due to the active transport of the neuropeptide CGRP to nerve terminals. In contrast, mCherry fused with the μ-opioid receptor does not seem to label fine nerve axons in the colorectum (45, 46). Collectively, it appears that efficient labeling of fine nerve axons in the colorectum can be achieved by tagging the fluorescent markers with proteins that are either membrane-bound (e.g., ChR2) or efficiently transported to the terminal axoplasm (e.g., CGRP in sensory afferents). Using sparse anterograde tracing from lumbosacral DRG, Spencer et al. (27) reported that 6% of the colorectal afferents had laminar endings, i.e., the submucosal and rectal intraganglionic laminar endings (IGLEs). We did not detect any laminar endings in the colorectum of VGLUT2/ChR2 mice, which likely reflects the following limitations of the current approach. First, VGLUT2-Cre promoter can only label 78% of the colorectal afferents and may have missed the small IGLE population. Second, the channelrhodopsin protein may fail to be transported to the IGLE structure of nerve endings. In addition, the VGLUT2-Cre promoter will also label a small fraction of myenteric neurons to confound the studies on extrinsic afferents.

Because of the low thickness of serosal and longitudinal muscular layers in mice, the myenteric plexuses can be imaged from the serosal side in uncleared whole mount colorectum as shown here (Fig. 1*C*) and in prior reports from others, e.g., (45). However, the colorectum is not transparent and can scatter 81% of the light passing through the wall (47), which leads to poor signal-to-noise ratios for detecting fine nerve fibers in deeper layers from the serosal side. To allow quantification of nerve fibers in deeper layers like the mucosa and submucosa, we adopted a tissue clearing SeeDB protocol originally developed for brain tissue to clear our fixed colorectal samples. The SeeDB protocol is based upon matching the refractive index between sample tissue and microscope glass by soaking the samples in a fructose solution (30). Similar to SeeDB, another tissue clearing approach of matching the refractive index was implemented to visualize mouse intestinal mucosa with subcellular-level resolution (47). However, technical details are lacking on the proprietary clearing reagent (FocusClear) used in that study.

We are aware of other optical tissue clearing protocols, which require dehydration (DABB), hyperhydration [ScaleA2 (48)] or forming a tissue-gel hybrid [CLARITY (49)] for removing lipids (50). The SeeDB and ScaleA2 protocol have been successfully employed in another study for reconstruction of murine colorectal mucosa (48). The DABB is also recently adopted to clear human colon (~1,000 μm thick) (51). However, the SeeDB appears to have much less impact on the bulk tissue geometry in contrast to the apparent tissue shrinkage (DABB) or expansion (ScaleA2, CLARITY) from other approaches (52). Thus, the SeeDB method used in current study likely allows a more precise detection of nerve fiber density and linearity index in the colorectum. Successful clearing of the colorectum by SeeDB for visualization of fine nerve fibers will likely trigger a wider application of this low-cost and convenient approach in neuro-gastrointestinal research.

Quantification of nerve fiber densities via vector path tracing revealed presence of VGLUT2-positive nerve fibers in all layers of the colorectum except the serosal and longitudinal muscular layers. This is consistent with the reported proportions of afferent axons in the colorectum from a tracing study in descending order of prevalence, submucosal (32%), circular muscular (25%), myenteric ganglia (22%), mucosal (11%), and longitudinal muscular layers (1%) (27). The current study and prior reports confirm the presence of a high density of extrinsic afferent fibers in the submucosa, which we have recently shown is the load-bearing structure of the colorectum (32, 33). More importantly, we describe for the first time presence of a large number of submucosal VGLUT2-positive nerve fibers with a curvy appearance, which maintain their average *LnIdx* (1.47) even when the colorectal wall is "unfolded" by 20 mmHg intraluminal pressure before tissue fixation. The meaning of this "curviness" remains unknown. One may hypothesize that the persistence of such morphology in most submucosal fibers when mechanical stimuli reach 20 mmHg would suggest that they not engage in encoding mechanical stimuli below 20 mmHg intraluminal pressure. Moreover, the strategical location of those curvy submucosal nerve fibers at the load-bearing region of the colorectum strongly suggests their role in nociceptive processing.

We also documented here a significant reduction in VGLUT2-positive nerve fiber density at *day 7* post-TNBS with recovery of fiber density at *day 28* post-TNBS. This agrees with our prior study using the pan-neuronal marker PGP 9.5, where we observed a pronounced reduction in the number of nerve fibers throughout the colorectum from *day 2* to *day 14* post-TNBS; recovery was complete at *day 28* post-TNBS (11). We noticed that VGLUT2-positive fibers only partially recovered to control levels in the mucosal and submucosal layers of the colonic segment, and in the mucosal layer of the intermediate segment. This is consistent with the significantly reduced neural encoding of colorectal stretch by muscular-mucosal afferents at *day 28* post-TNBS, which presumably have endings in the mucosal and submucosal layers of the colorectum (11).

We also reported that 9.90% to 15.98% of submucosal afferents exhibited pronounced curviness ($LnIdx > 1.67$), rendering them unlikely to encode even noxious colorectal distension under normal physiological conditions. Interestingly, the proportions of those pronounced curvy fibers showed considerable reduction to 3.92%–8.70% at *day 7* post-TNBS and did not recover to control at *day 28* in the rectal segment (4.07%). Coincidently, our prior functional characterization of mechanically insensitive afferents (MIA) showed a similar change in proportion following TNBS treatment, i.e., a significant reduction in the proportion of MIAs following TNBS treatment without recovery even at *day 28* post-TNBS (11). This may suggest that those pronounced curvy fibers in the submucosa are MIAs, portions of which are persistently sensitized to mechanical stimuli by reducing their curviness or *LnIdx* following TNBS treatment.

In conclusion, we implemented a macro-level labeling strategy using VGLUT2-Cre mice to fluorescently tag most of the extrinsic afferent fibers in the colorectum using membrane-bound ChR2. We adopted an optical tissue clearing protocol (SeeDB) to allow visualization of fine nerve fibers in whole mount colorectum. Vector path tracing of individual nerve fibers reveals widespread presence of VGLUT2-positive nerve fibers in all layers of the colorectum except the serosal and longitudinal muscular layers. Intracolonic TNBS treatment significantly reduced VGLUT2-positive nerve tissue density in submucosal, myenteric plexus, and mucosal layers, which mostly recovered to control levels 28 days after TNBS instillation. VGLUT2-positive fibers in the colonic mucosa and submucosa (as well as intermediate mucosa) did not fully recover to control levels on *day 28* post-TNBS, which might account for the reduced neural encoding by muscular-mucosal afferents post-TNBS (11). VGLUT2-positive fibers in the submucosa were meandering and curvy, with ~10% of those fibers demonstrating pronounced curviness ($LnIdx > 1.67$). The proportion of pronounced curvy fibers in the submucosa was reduced following intracolonic TNBS treatment and did not recover in rectal segments, as seen 28 days after treatment, consistent with the persistent sensitization of mechanically insensitive afferents (MIAs) even 28 days after TNBS treatment. Outcomes of this study draw focused attention to changes in afferent morphology in the colorectum as potentially contributing factors to sensitization of mechanosensitive and mechanically insensitive afferents.

ACKNOWLEDGMENTS

We sincerely thank Dr. Jerry Gebhart for critically reviewing and editing the manuscript.

GRANTS

This research is supported by National Institutes of Health Grant R01 DK120824 awarded to B. Feng and Grant R01DC014044 awarded to M. Han.

DISCLOSURES

No conflicts of interest, financial or otherwise, are declared by the authors.

AUTHOR CONTRIBUTIONS

B.F. conceived and designed research; T.G., S.P., D.S., L.C., S.E., and B.F. performed experiments; T.G., S.P., D.S., L.C., M.H., P.R.B., and B.F. analyzed data; T.G., S.P., L.C., S.E., D.M.P., and B.F. interpreted results of experiments; T.G., S.P., L.C., and B.F. prepared figures; T.G. and B.F. drafted manuscript; T.G., S.P., D.S., L.C., S.E., D.M.P., M.H., P.R.B., and B.F. edited and revised manuscript; T.G., S.P., D.S., L.C., S.E., D.M.P., M.H., P.R.B., and B.F. approved final version of manuscript.

REFERENCES

1. **Verne GN**, **Robinson ME**, **Price DD.** Hypersensitivity to visceral and cutaneous pain in the irritable bowel syndrome. *Pain* 93: 7–14, 2001. doi:10.1016/S0304-3959(01)00285-8.
2. **Feng B**, **La JH**, **Schwartz ES**, **Gebhart GF.** Irritable bowel syndrome: methods, mechanisms, and pathophysiology. Neural and neuroimmune mechanisms of visceral hypersensitivity in irritable bowel syndrome. *Am J Physiol Gastrointest Liver Physiol* 302: G1085–G1098, 2012. doi:10.1152/ajpgi.00542.2011.
3. **Price DD**, **Craggs JG**, **Zhou Q**, **Verne GN**, **Perlstein WM**, **Robinson ME.** Widespread hyperalgesia in irritable bowel syndrome is dynamically maintained by tonic visceral impulse input and placebo/nocebo factors: evidence from human psychophysics, animal models, and neuroimaging. *Neuroimage* 47: 995–1001, 2009. doi:10.1016/j.neuroimage.2009.04.028.
4. **Verne GN**, **Robinson ME**, **Vase L**, **Price DD.** Reversal of visceral and cutaneous hyperalgesia by local rectal anesthesia in irritable bowel syndrome (IBS) patients. *Pain* 105: 223–230, 2003. doi:10.1016/s0304-3959(03)00210-0.
5. **Verne GN**, **Sen A**, **Price DD.** Intrarectal lidocaine is an effective treatment for abdominal pain associated with diarrhea-predominant irritable bowel syndrome. *J Pain* 6: 493–496, 2005. doi:10.1016/j.jpain.2005.02.009.
6. **Hughes PA**, **Brierley SM**, **Martin CM**, **Brookes SJ**, **Linden DR**, **Blackshaw LA.** Post-inflammatory colonic afferent sensitisation: different subtypes, different pathways and different time courses. *Gut* 58: 1333–1341, 2009 [Erratum in *Gut* 60: 140, 2011]. doi:10.1136/gut.2008.170811.
7. **La JH**, **Feng B**, **Schwartz ES**, **Brumovsky PR**, **Gebhart GF.** Luminal hypertonicity and acidity modulate colorectal afferents and induce persistent visceral hypersensitivity. *Am J Physiol Gastrointest Liver Physiol* 303: G802–G809, 2012. doi:10.1152/ajpgi.00259.2012.
8. **Robinson DA**, **Calejesan AA**, **Wei F**, **Gebhart GF**, **Zhuo M.** Endogenous facilitation: from molecular mechanisms to persistent pain. *Curr Neurovasc Res* 1: 11–20, 2004 [Erratum in *Curr Neurovasc Res* 1: 191, 2004]. doi:10.2174/1567202043480189.
9. **Shinoda M**, **Feng B**, **Gebhart GF.** Peripheral and central P2X receptor contributions to colon mechanosensitivity and hypersensitivity in the mouse. *Gastroenterology* 137: 2096–2104, 2009. doi:10.1053/j.gastro.2009.06.048.
10. **Tanaka T**, **Shinoda M**, **Feng B**, **Albers KM**, **Gebhart GF.** Modulation of visceral hypersensitivity by glial cell line-derived neurotrophic factor family receptor α-3 in colorectal afferents. *Am J Physiol Gastrointest Liver Physiol* 300: G418–G424, 2011. doi:10.1152/ajpgi.00456.2010.
11. **Feng B**, **La JH**, **Tanaka T**, **Schwartz ES**, **McMurray TP**, **Gebhart GF.** Altered colorectal afferent function associated with TNBS-induced visceral hypersensitivity in mice. *Am J Physiol Gastrointest Liver Physiol* 303: G817–G824, 2012. doi:10.1152/ajpgi.00257.2012.
12. **Schwille-Kiuntke J**, **Mazurak N**, **Enck P.** Systematic review with meta-analysis: post-infectious irritable bowel syndrome after travellers' diarrhoea. *Aliment Pharmacol Ther* 41: 1029–1037, 2015. doi:10.1111/apt.13199.
13. **Feng B**, **Guo T.** Visceral pain from colon and rectum: the mechanotransduction and biomechanics. *J Neural Transm (Vienna)* 127: 415–429, 2020. doi:10.1007/s00702-019-02088-8.
14. **Brierley SM**, **Jones RC 3rd**,**Gebhart GF**, **Blackshaw LA.** Splanchnic and pelvic mechanosensory afferents signal different qualities of colonic stimuli in mice. *Gastroenterology* 127: 166–178, 2004. doi:10.1053/j.gastro.2004.04.008.
15. **Feng B**, **Gebhart GF.** Characterization of silent afferents in the pelvic and splanchnic innervations of the mouse colorectum. *Am J Physiol Gastrointest Liver Physiol* 300: G170–G180, 2011. doi:10.1152/ajpgi.00406.2010.
16. **Feng B**, **Gebhart GF.** In vitro functional characterization of mouse colorectal afferent endings. *J Vis Exp*: 52310, 2015. doi:10.3791/52310.
17. **Feng B**, **Joyce SC**, **Gebhart GF.** Optogenetic activation of mechanically insensitive afferents in mouse colorectum reveals chemosensitivity. *Am J Physiol Gastrointest Liver Physiol* 310: G790–G798, 2016. doi:10.1152/ajpgi.00430.2015.
18. **Feng B**, **Zhu Y**, **La JH**, **Wills ZP**, **Gebhart GF.** Experimental and computational evidence for an essential role of NaV1.6 in spike initiation at stretch-sensitive colorectal afferent endings. *J Neurophysiol* 113: 2618–2634, 2015. doi:10.1152/jn.00717.2014.
19. **Ibeakanma C**, **Miranda-Morales M**, **Richards M**, **Bautista-Cruz F**, **Martin N**, **Hurlbut D**, **Vanner S.** *Citrobacter rodentium* colitis evokes post-infectious hyperexcitability of mouse nociceptive colonic dorsal root ganglion neurons. *J Physiol* 587: 3505–3521, 2009. doi:10.1113/jphysiol.2009.169110.
20. **McGuire C**, **Boundouki G**, **Hockley JRF**, **Reed D**, **Cibert-Goton V**, **Peiris M**, **Kung V**, **Broad J**, **Aziz Q**, **Chan C**, **Ahmed S**, **Thaha MA**, **Sanger GJ**, **Blackshaw LA**, **Knowles CH**, **Bulmer DC.** Ex vivo study of human visceral nociceptors. *Gut* 67: 86–96, 2018. doi:10.1136/gutjnl-2016-311629.
21. **Zagorodnyuk VP**, **Lynn P**, **Costa M**, **Brookes SJ.** Mechanisms of mechanotransduction by specialized low-threshold mechanoreceptors in the guinea pig rectum. *Am J Physiol Gastrointest Liver Physiol* 289: G397–G406, 2005. doi:10.1152/ajpgi.00557.2004.
22. **Hibberd TJ**, **Kestell GR**, **Kyloh MA**, **Brookes SJ**, **Wattchow DA**, **Spencer NJ.** Identification of different functional types of spinal afferent neurons innervating the mouse large intestine using a novel CGRPalpha transgenic reporter mouse. *Am J Physiol Gastrointest Liver Physiol* 310: G561–G573, 2016. doi:10.1152/ajpgi.00462.2015.
23. **Malin SA**, **Christianson JA**, **Bielefeldt K**, **Davis BM.** TPRV1 expression defines functionally distinct pelvic colon afferents. *J Neurosci* 29: 743–752, 2009. doi:10.1523/JNEUROSCI.3791-08.2009.
24. **Guo T**, **Bian Z**, **Trocki K**, **Chen L**, **Zheng G**, **Feng B.** Optical recording reveals topological distribution of functionally classified colorectal afferent neurons in intact lumbosacral DRG. *Physiol Rep* 7: e14097, 2019. doi:10.14814/phy2.14097.
25. **Zhu Y**, **Feng B**, **Schwartz ES**, **Gebhart GF**, **Prescott SA.** Novel method to assess axonal excitability using channelrhodopsin-based photoactivation. *J Neurophysiol* 113: 2242–2249, 2015. doi:10.1152/jn.00982.2014.
26. **Spencer NJ**, **Kerrin A**, **Singer CA**, **Hennig GW**, **Gerthoffer WT**, **McDonnell O.** Identification of capsaicin-sensitive rectal mechanoreceptors activated by rectal distension in mice. *Neuroscience* 153: 518–534, 2008. doi:10.1016/j.neuroscience.2008.02.054.
27. **Spencer NJ**, **Kyloh M**, **Duffield M.** Identification of different types of spinal afferent nerve endings that encode noxious and innocuous stimuli in the large intestine using a novel anterograde tracing technique. *PLoS One* 9: e112466, 2014. doi:10.1371/journal.pone.0112466.
28. **Malet M**, **Vieytes CA**, **Lundgren KH**, **Seal RP**, **Tomasella E**, **Seroogy KB**, **Hokfelt T**, **Gebhart GF**, **Brumovsky PR.** Transcript expression of vesicular glutamate transporters in lumbar dorsal root ganglia and the

spinal cord of mice - effects of peripheral axotomy or hindpaw inflammation. *Neuroscience* 248: 95–111, 2013. doi:10.1016/j.neuroscience.2013.05.044.

29. **Brumovsky PR**, **Robinson DR**, **La JH**, **Seroogy KB**, **Lundgren KH**, **Albers KM**, **Kiyatkin ME**, **Seal RP**, **Edwards RH**, **Watanabe M**, **Hokfelt T**, **Gebhart GF.** Expression of vesicular glutamate transporters type 1 and 2 in sensory and autonomic neurons innervating the mouse colorectum. *J Comp Neurol* 519: 3346–3366, 2011. doi:10.1002/cne.22730.
30. **Ke MT**, **Fujimoto S**, **Imai T.** SeeDB: a simple and morphology-preserving optical clearing agent for neuronal circuit reconstruction. *Nat Neurosci* 16: 1154–1161, 2013. doi:10.1038/nn.3447.
31. **Feng B**, **Brumovsky PR**, **Gebhart GF.** Differential roles of stretch-sensitive pelvic nerve afferents innervating mouse distal colon and rectum. *Am J Physiol Gastrointest Liver Physiol* 298: G402–G409, 2010. doi:10.1152/ajpgi.00487.2009.
32. **Siri S**, **Maier F**, **Chen L**, **Santos S**, **Pierce DM**, **Feng B.** Differential biomechanical properties of mouse distal colon and rectum innervated by the splanchnic and pelvic afferents. *Am J Physiol Gastrointest Liver Physiol* 316: G473–G481, 2019. doi:10.1152/ajpgi.00324.2018.
33. **Siri S**, **Maier F**, **Santos S**, **Pierce DM**, **Feng B.** The load-bearing function of the colorectal submucosa and its relevance to visceral nociception elicited by mechanical stretch. *Am J Physiol Gastrointest Liver Physiol* 317: G349–G358, 2019. doi:10.1152/ajpgi.00127.2019.
34. **Yang B**, **Treweek JB**, **Kulkarni RP**, **Deverman BE**, **Chen CK**, **Lubeck E**, **Shah S**, **Cai L**, **Gradinaru V.** Single-cell phenotyping within transparent intact tissue through whole-body clearing. *Cell* 158: 945–958, 2014. doi:10.1016/j.cell.2014.07.017.
35. **Delvalle NM**, **Dharshika C**, **Morales-Soto W**, **Fried DE**, **Gaudette L**, **Gulbransen BD.** Communication between enteric neurons, glia, and nociceptors underlies the effects of tachykinins on neuroinflammation. *Cell Mol Gastroenterol Hepatol* 6: 321–344, 2018. doi:10.1016/j.jcmgh.2018.05.009.
36. **Longair MH**, **Baker DA**, **Armstrong JD.** Simple neurite tracer: open source software for reconstruction, visualization and analysis of neuronal processes. *Bioinformatics* 27: 2453–2454, 2011. doi:10.1093/bioinformatics/btr390.
37. **Brumovsky PR**, **Seroogy KB**, **Lundgren KH**, **Watanabe M**, **Hokfelt T**, **Gebhart GF.** Some lumbar sympathetic neurons develop a glutamatergic phenotype after peripheral axotomy with a note on VGLUT-positive perineuronal baskets. *Exp Neurol* 230: 258–272, 2011. doi:10.1016/j.expneurol.2011.05.004.
38. **Maier F**, **Siri S**, **Santos S**, **Chen L**, **Feng B**, **Pierce DM.** The heterogeneous morphology of networked collagen in distal colon and rectum of mice quantified via nonlinear microscopy. *J Mech Behav Biomed Mater* 113: 104116, 2021. doi:10.1016/j.jmbbm.2020.104116.
39. **Brookes SJ**, **Spencer NJ**, **Costa M**, **Zagorodnyuk VP.** Extrinsic primary afferent signalling in the gut. *Nat Rev Gastroenterol Hepatol* 10: 286–296, 2013. doi:10.1038/nrgastro.2013.29.
40. **Brumovsky PR**, **La JH**, **Gebhart GF.** Distribution across tissue layers of extrinsic nerves innervating the mouse colorectum - an in vitro anterograde tracing study. *Neurogastroenterol Motil* 26: 1494–1507, 2014. doi:10.1111/nmo.12419.
41. **Zagorodnyuk VP**, **Brookes SJ**, **Spencer NJ.** Structure-function relationship of sensory endings in the gut and bladder. *Auton Neurosci* 153: 3–11, 2010. doi:10.1016/j.autneu.2009.07.018.
42. **Spencer NJ**, **Magnusdottir EI**, **Jakobsson JET**, **Kestell G**, **Chen BN**, **Morris D**, **Brookes SJ**, **Lagerstrom MC.** CGRPalpha within the Trpv1-Cre population contributes to visceral nociception. *Am J Physiol Gastrointest Liver Physiol* 314: G188–G200, 2018. doi:10.1152/ajpgi.00188.2017.
43. **Spencer NJ**, **Sorensen J**, **Travis L**, **Wiklendt L**, **Costa M**, **Hibberd T.** Imaging activation of peptidergic spinal afferent varicosities within visceral organs using novel CGRPα-mCherry reporter mice. *Am J Physiol Gastrointest Liver Physiol* 311: G880–G894, 2016. doi:10.1152/ajpgi.00250.2016.
44. **Christianson JA**, **Traub RJ**, **Davis BM.** Differences in spinal distribution and neurochemical phenotype of colonic afferents in mouse and rat. *J Comp Neurol* 494: 246–259, 2006. doi:10.1002/cne.20816.
45. **DiCello JJ**, **Carbone SE**, **Saito A**, **Rajasekhar P**, **Ceredig RA**, **Pham V**, **Valant C**, **Christopoulos A**, **Veldhuis NA**, **Canals M**, **Massotte D**, **Poole DP.** Mu and delta opioid receptors are coexpressed and functionally interact in the enteric nervous system of the mouse colon. *Cell Mol Gastroenterol Hepatol* 9: 465–483, 2020. doi:10.1016/j.jcmgh.2019.11.006.
46. **Feng B.** New insights on expression and function of Mu and delta opioid receptors in mouse gastrointestinal tract. *Cell Mol Gastroenterol Hepatol* 9: 553–554, 2020. doi:10.1016/j.jcmgh.2020.01.001.
47. **Fu YY**, **Lin CW**, **Enikolopov G**, **Sibley E**, **Chiang AS**, **Tang SC.** Microtome-free 3-dimensional confocal imaging method for visualization of mouse intestine with subcellular-level resolution. *Gastroenterology* 137: 453–465, 2009. doi:10.1053/j.gastro.2009.05.008.
48. **Liu CY**, **Dube PE**, **Girish N**, **Reddy AT**, **Polk DB.** Optical reconstruction of murine colorectal mucosa at cellular resolution. *Am J Physiol Gastrointest Liver Physiol* 308: G721–G735, 2015. doi:10.1152/ajpgi.00310.2014.
49. **Jensen KHR**, **Berg RW.** Advances and perspectives in tissue clearing using CLARITY. *J Chem Neuroanat* 86: 19–34, 2017. doi:10.1016/j.jchemneu.2017.07.005.
50. **Seo J**, **Choe M**, **Kim SY.** Clearing and labeling techniques for large-scale biological tissues. *Mol Cells* 39: 439–446, 2016. [Erratum in *Mol Cells* 42: 96, 2019]. doi:10.14348/molcells.2016.0088.
51. **Graham KD**, **López SH**, **Sengupta R**, **Shenoy A**, **Schneider S**, **Wright CM**, **Feldman M**, **Furth E**, **Valdivieso F**, **Lemke A**, **Wilkins BJ**, **Naji A**, **Doolin EJ**, **Howard MJ**, **Heuckeroth RO.** Robust, 3-dimensional visualization of human colon enteric nervous system without tissue sectioning. *Gastroenterology* 158: 2221–2235, 2020. doi:10.1053/j.gastro.2020.02.035.
52. **Richardson DS**, **Lichtman JW.** Clarifying tissue clearing. *Cell* 162: 246–257, 2015. doi:10.1016/j.cell.2015.06.067.